Walking droplets in a circular corral: Quantisation and chaos

Walking droplets in a circular corral: Quantisation and chaos

Tudor Cristea-Platon, Pedro J. Sáenz, and John W. M. Bush

Citation: Chaos **28**, 096116 (2018); doi: 10.1063/1.5034123
View online: https://doi.org/10.1063/1.5034123
View Table of Contents: http://aip.scitation.org/toc/cha/28/9
Published by the American Institute of Physics

Walking droplets in a circular corral: Quantisation and chaos

Tudor Cristea-Platon, Pedro J. Sáenz, and John W. M. Bush
Department of Mathematics, Massachusetts Institute of Technology, 77 Massachusetts Avenue, Cambridge, Massachusetts 02139, USA

(Received 9 April 2018; accepted 12 August 2018; published online 24 September 2018)

A millimetric liquid droplet may walk across the surface of a vibrating liquid bath through a resonant interaction with its self-generated wavefield. Such walking droplets, or "walkers," have attracted considerable recent interest because they exhibit certain features previously believed to be exclusive to the microscopic, quantum realm. In particular, the intricate motion of a walker confined to a closed geometry is known to give rise to a coherent wave-like statistical behavior similar to that of electrons confined to quantum corrals. Here, we examine experimentally the dynamics of a walker inside a circular corral. We first illustrate the emergence of a variety of stable dynamical states for relatively low vibrational accelerations, which lead to a double quantisation in angular momentum and orbital radius. We then characterise the system's transition to chaos for increasing vibrational acceleration and illustrate the resulting breakdown of the double quantisation. Finally, we discuss the similarities and differences between the dynamics and statistics of a walker inside a circular corral and that of a walker subject to a simple harmonic potential. *Published by AIP Publishing.* https://doi.org/10.1063/1.5034123

Small liquid droplets may walk across the surface of a vertically vibrated liquid bath, driven by interactions with their own wave fields. The walking-droplet system has given rise to the field of pilot-wave hydrodynamics, which has established macroscopic analogues of a number of quantum phenomena, including tunnelling, wave-like statistics of particles in confined geometries, and orbital quantisation. Confining walking droplets with a simple harmonic potential leads to a variety of periodic, quasi-periodic, and chaotic trajectories that emerge successively as the vibrational forcing is increased. Experiments have demonstrated that walking droplets confined to circular and elliptical corrals display chaotic motion at large vibrational forcing; however, their motion at low forcing has received relatively little attention. Here, we present an experimental investigation of the dynamics of walking droplets confined to a circular corral. We focus on characterising the emergence of periodic and quasi-periodic trajectories at low forcing and the transition to the chaotic regime as the forcing is increased progressively. We compare the droplet trajectories to their counterparts in the simple harmonic potential.

INTRODUCTION

Couder and co-workers[1,2] discovered that a small liquid droplet can walk above the free surface of a vibrating liquid bath, self-propelled via a resonant interaction with its own wavefield. Since their discovery more than a decade ago, these walking droplets have received considerable attention owing to their ability to exhibit behaviors analogous to those observed in a number of quantum systems (see review of Bush)[3]. The quantum-like behavior in the walking droplet system typically emerges as the bath's vibrational acceleration γ approaches the Faraday threshold γ_F, the critical vibrational acceleration above which the fluid bath destabilises into a field of standing subharmonic waves.[4] A crucial parameter in the walker system is the so-called "memory," defined as γ/γ_F, which provides a measure of the proximity to the Faraday threshold and so the longevity of the waves excited by the bouncing drop at each impact.[5] In the high-memory regime, the waves generated by each impact are relatively persistent; consequently, the walker's motion is more strongly influenced by its past.

Harris *et al.*[6] investigated the motion of a walker confined to a circular cavity or "corral." They found that at low and intermediate memories ($0.82 < \gamma/\gamma_F < 0.94$), the walker may display simple periodic trajectories. They focused their study on the emergence of a wave-like statistical behavior in the high-memory limit. Specifically, they found that the seemingly chaotic motion of the drop eventually leads to a probability distribution related to the most unstable wave mode of the cavity, which is reminiscent of the probability distribution of a two-dimensional electron gas confined to a circular quantum corral.[7] Reproducing this robust statistical behavior with theoretical models[8–11] has proven to be challenging, owing largely to the subtleties of walker-boundary interactions.[12]

Sáenz *et al.*[13] recently considered the dynamics of a walking drop in a relatively shallow elliptical corral. Owing to the special properties of this geometry, the authors demonstrated that a localised topological inhomogeneity inside the corral may lead to resonant projection effects in the walker's statistics analogous to those observed in elliptical quantum corrals.[14–16] In particular, the authors found that an inhomogeneity in the corral, in the form of a submerged circular well, may drive the walker to excite specific elliptical eigenmodes that result in drastic changes in the particle's statistical behavior, as do magnetic impurities in the quantum corral. Finally, they demonstrated the emergence of a coherent mean

(time-averaged) wave field with a form similar to the droplet's position histogram.

While the corral experiments sought to elucidate the statistical behavior of walking drops confined by solid boundaries, other investigations have characterised and rationalised the dynamics of walkers confined by central forces. Perrard *et al.*[17,18] performed experiments with ferro-fluid suspended within a droplet. By subjecting this walker to a vertical magnetic field with a radial gradient, they studied the effects of a confining simple harmonic potential on a walking droplet. The authors reported the existence of both stable and chaotic trajectories and the emergence of a double quantisation in orbital radius and angular momentum over a certain span of memories. Their experiments thus demonstrate a classical analog of the quantum mechanical eigenstates of the simple harmonic potential, as are defined in terms of their quantised energy and angular momentum.

The original experiments by Perrard *et al.*[17,18] have motivated a number of theoretical developments. Labousse *et al.*[19] analyzed the motion of a walker in an attractive potential and argued that the horizontal motion may be characterised in terms of three distinct time scales at high memory, associated with droplet propulsion on a straight-line, motion along a pivot with a preferred radius of curvatures, and self-organisation into a global wave structure associated with a periodic or quasi-periodic orbit. Labousse *et al.*[20] investigated the stability of the circular orbits arising at low memory and so rationalised the corresponding quantisation of orbital radius. Durey *et al.*[21] developed a relatively sophisticated method to analyze the drop's trajectory in terms of stable sub-trajectories, which allowed the authors to demonstrate that the double quantisation of orbital radius and angular momentum occurs even in the high-memory regime, where the dynamics are dominated by erratic switching between unstable periodic and quasi-periodic sub-trajectories. Kurianski *et al.*[22] revisited this system theoretically with the stroboscopic model of Oza *et al.*[23] and captured a number of periodic, quasi-periodic, and chaotic walker trajectories, including a number that were not reported experimentally. Kurianski *et al.* also demonstrated that a requirement for double quantisation in the simple harmonic potential system is that the memory time (the characteristic decay time of the Faraday waves) exceeds the crossing time (the characteristic time taken for the drop to span its maximum range). Their study concludes with the observation that the specific details of the double quantisation identified in the hydrodynamic pilot-wave system are weakly sensitive to the specifics of the wave model used.

A common feature of walker motion in corrals and a simple harmonic potential is the presence of chaos. Tambasco *et al.*[24] were the first to characterise theoretically the onset of chaos in orbital pilot-wave dynamics. The authors considered the dynamics of walking droplets acted upon by external forces such as Coriolis, Coulomb, and linear spring forces. They demonstrated that the route to chaos followed in the destabilisation of circular orbits depends on the form of the external force. For the case of Coulomb and Coriolis forces, chaos sets in via a classic period-doubling cascade.[25,26] In the case of a central harmonic potential, the route to chaos is reminiscent of the Ruelle-Takens-Newhouse scenario.[27,28]

Gilet developed a discrete theoretical model[9,10] of walkers in circular corrals that captures the family of stable circular orbits arising at low memory reported by Harris *et al.*,[6] as well as chaotic behavior at higher memory. The transition to chaos with increasing memory was also characterised in terms of a supercritical Neimark-Sacker bifurcation. Rahman and Blackmore[29] build upon these model results for the special case of one-dimensional motion and demonstrated that both supercritical and subcritical Neimark-Sacker bifurcations may arise. In the high memory limit, Gilet's model[9,10] predicts trajectories with cusps at which the walker stops and then restarts in a different direction. These sharp turning events occur at radii corresponding to the extrema of the axially symmetric wave eigenmode and so are separated by approximately half of the Faraday wavelength.

While walking drops in corrals[6,9,10,13,29] and harmonic potentials[17–22] are two of the more robust and rich examples of hydrodynamic quantum analogs, to date these two systems have been treated separately. Thinking of the circular corral walls as an alternative means of inducing a radial potential on a walking droplet allows one to place these systems on equal footing. Building upon the works of Harris *et al.*[6] and Sáenz *et al.*,[13] we thus revisit the circular corral experiments to illustrate the emergence of a variety of dynamical states, stable at low memory and unstable at high, that lead to a double quantisation in the angular momentum and orbital radius reminiscent of that reported in the simple harmonic potential.[17] In addition, we characterise the system's transition to chaos with increasing vibrational acceleration and discuss the concomitant disappearance of the double quantisation.

EXPERIMENTS

A schematic of the experimental setup is shown in Fig. 1(a). A circular corral made out of acrylic is filled with silicon oil with density $\rho = 950\,\mathrm{kg\,m^{-3}}$, viscosity $\nu = 20.9\,\mathrm{cSt}$, and surface tension $\sigma = 20.6\,\mathrm{mN\,m^{-1}}$. The bath is mounted on an optical table and vibrated vertically by an electromagnetic shaker with acceleration $\Gamma(t) = \gamma\cos(\omega t)$, where γ and $f = \omega/2\pi = 80\,\mathrm{Hz}$ are the prescribed maximum acceleration and frequency, respectively. The circular corral of diameter $D = 20.2\,\mathrm{mm}$ is filled to a height $h = 5.92 \pm 0.05\,\mathrm{mm}$ such that a very thin liquid film of depth $h_1 = 0.22 \pm 0.03\,\mathrm{mm}$ overlays its border, serving as a wave damper. The ratio of the cavity diameter to the Faraday wavelength is 4.25.

The shaker was connected to the bath by a thin steel rod coupled to a linear air bearing in order to ensure a spatially uniform vibration to within 0.1%.[30] The forcing was monitored by two accelerometers, attached to the bath on opposite sides of the drive shaft, and a closed-loop feedback ensured a constant acceleration amplitude to within $\pm 0.002\,\mathrm{g}$.[30] A droplet of the same silicon oil of diameter $d = 0.70 \pm 0.01\,\mathrm{mm}$ was generated with a piezoelectric droplet-on-demand generator and placed on the vibrating bath with the help of a removable slide.[31] To ensure that ambient air currents did not affect the results, the corral was sealed with a transparent acrylic lid.[32] The image acquisition was done using a charge-coupled device (CCD) camera mounted

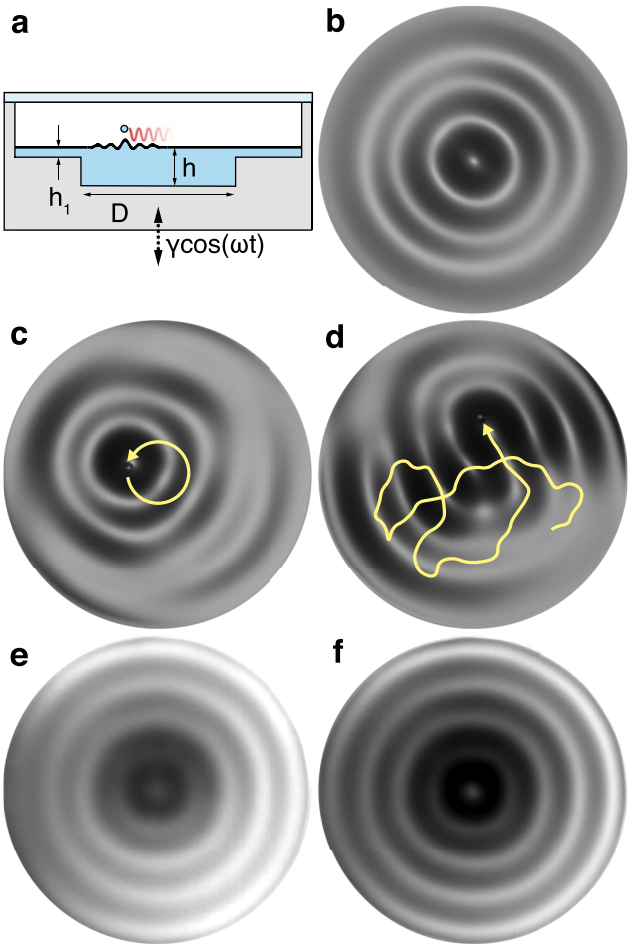

FIG. 1. Experimental setup.[6] (a) Cross-sectional view of the circular corral filled with silicon oil. (b) Faraday wave pattern obtained for the circular corral driven at $f = 80$ Hz and $\gamma = 1.01\gamma_F$. Examples of the walker trajectory (of duration ~ 8 s) and instantaneous wave form at (c) $\gamma/\gamma_F = 0.91$ and (d) $\gamma/\gamma_F = 0.99$. The corresponding mean wave form (obtained over ~ 60 s) at (e) $\gamma/\gamma_F = 0.91$ and (f) 0.99, respectively.

directly above the bath operating at 20 frames per second. The bath was illuminated with a light-emitting diode (LED) light ring to increase the contrast between the drop and the black background. The walker's location was extracted using an in-house particle-tracking algorithm.

For γ just above the Faraday threshold γ_F (which depends on f and h, the fluid properties and cavity size), the bath displays the wave pattern shown in Fig. 1(b), corresponding to the most unstable Faraday wave mode of the cavity. This wave form is visualised using the normal reflection of light from the free surface,[33] measurement of which required a semi-reflective mirror angled at 45° between the CCD camera and the bath, and a diffuse-light lamp facing the mirror and illuminating the bath.[13] The same technique was used to compute the instantaneous wave fields [e.g., Figs. 1(c) and 1(d)], the averaging of which yielded the mean wave fields [Figs. 1(e) and 1(f)].

Figures 1(c) and 1(d) illustrate the instantaneous wave form and the associated droplet trajectory for two different memory values. At $\gamma/\gamma_F = 0.91$, the droplet follows a circular orbit centred on the corral [Fig. 1(c)]. At $\gamma/\gamma_F = 0.99$, the motion is irregular, with many abrupt changes in direction and speed [Fig. 1(d)]. The instantaneous wave form generally becomes more complex as the memory is increased. Figures 1(e) and 1(f) illustrate the mean wave forms obtained by superposing with equal weights the instantaneous wave forms over a 15 min interval.[13] Despite the drastically different walker behavior, we note the striking similarity between both of these waveforms and the most unstable Faraday wavemode of the cavity [Fig. 1(b)]. The features of the mean wave form become more pronounced at higher memories, as is consistent with the droplet dynamics being more strongly influenced by the mean wave field at higher memory.[34]

We study the walker's dynamics exclusively for $\gamma < \gamma_F$, so that no waves would exist in the absence of the droplet. For the range of parameters considered, $\gamma_F = 4.732 \pm 0.004g$. We increased the memory of the system from $\gamma/\gamma_F = 0.87$ to 0.99 in steps of $\delta\gamma/\gamma_F = 0.005$. Each experiment was recorded for a period of 5 min. The characteristic decay time of the subharmonic Faraday waves, or memory time $T_M = T_d/(1-\gamma/\gamma_F) \sim 0.1 - 2$ s, where $T_d \sim \lambda_F^2/(8\pi^2\nu)$ is the wave decay time in the absence of vibrational forcing, and λ_F is the Faraday wavelength as prescribed by the standard water-wave dispersion relation.[3] The droplet's characteristic orbital or crossing time $T_c = D/(2u) \sim 2 - 4$ s, where $u \sim 4.2 - 5.7\,\mathrm{mm\,s^{-1}}$ is the characteristic droplet speed in the range of memory under consideration. We note that these two time scales are comparable, indicating that we are in the memory-dominated regime in which the entirety of the bath surface is generally excited at all times.[22]

Fundamental trajectories and double quantisation

We proceed by detailing the evolution of the system with increasing memory for our small corral geometry. In relatively large domains, as γ is increased beyond the walking threshold, the stationary bouncing state gives way to rectilinear walking at a constant speed.[1,2,26,35] In our small circular corral, the onset of motion is decidedly different. Just above the walking threshold, $\gamma/\gamma_F = 0.85$, the droplet executes rectilinear oscillations of amplitude comparable to its diameter. At slightly higher memories, specifically, $\gamma/\gamma_F = 0.87$ [Fig. 2(a)], the walker reaches its first stable trajectory, the centred circle of radius $\sim 0.32\lambda_F$ shown in Fig. 1(c). Progressively increasing γ/γ_F to 0.90 leads to the continuous expansion of the orbital radius to a value of $\sim 0.44\lambda_F$. At $\gamma/\gamma_F = 0.91$, the circle begins to wobble and destabilise, with the droplet describing a deformed circular orbit of maximum radial extent $\sim 0.7\lambda_F$ [Fig. 2(b)]. The second stable trajectory is reached at $\gamma/\gamma_F = 0.92$, when the walker describes a centred circular orbit with radius $\sim 0.7\lambda_F$ [Fig. 2(c)]. We note that the small and large circular trajectories [Figs. 2(a) and 2(c)] roughly coincide, respectively, with the innermost and second innermost dark rings of the mean wave field evident in Figs. 1(e) and 1(f). Increasing the memory to $\gamma/\gamma_F = 0.93$ destabilises the larger circular orbits, leading to wobbling [Fig. 2(d)].

Following the destabilisation of the large orbit, relatively complex trajectories arise, of the form illustrated in Figs. 2(e)–2(g). As shown by Perrard *et al.*,[17] however, one may identify a variety of periodic and quasi-periodic

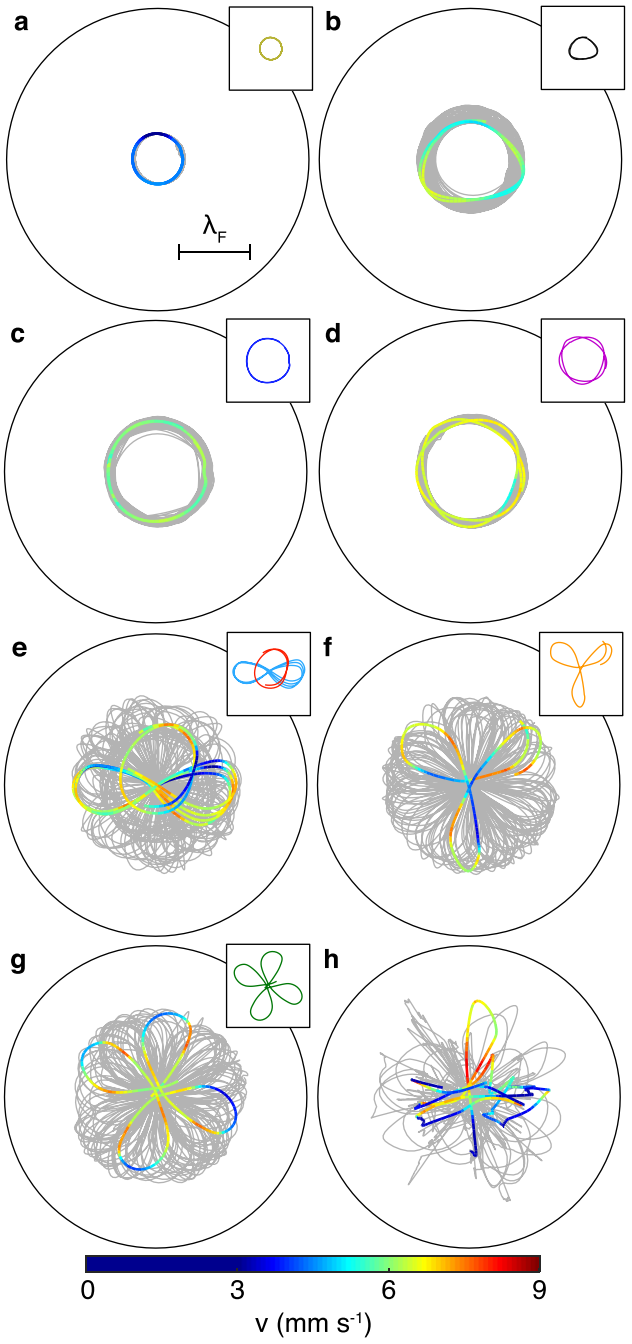

FIG. 2. Fundamental trajectories in a circular corral of diameter $D = 20.2$ mm. (a) Small circle at $\gamma/\gamma_F = 0.88$. (b) Deformed circle at $\gamma/\gamma_F = 0.91$. (c) Large circle at $\gamma/\gamma_F = 0.92$. (d) Large wobbling circle at $\gamma/\gamma_F = 0.93$. (e) Oval and lemniscate embedded within a complex trajectory at $\gamma/\gamma_F = 0.935$. (f) Trefoil at $\gamma/\gamma_F = 0.94$. (g) Papillon at $\gamma/\gamma_F = 0.95$. (h) Erratic motion punctuated by intermittent trapping at $\gamma/\gamma_F = 0.98$. Wave-induced trapping locations correspond to the deep blue portions of the trajectories. The fundamental trajectories are colour-coded according to instantaneous speed. The gray trajectories represent 5 min long series. $\lambda_F = 4.75$ mm indicates the Faraday wavelength.

sub-trajectories embedded within these complex trajectories, henceforth referred to as "fundamental trajectories," whose form depends on memory. At $\gamma/\gamma_F = 0.935$, we note the emergence of two fundamental trajectories, ovals, and lemniscates [Fig. 2(e)]. Further increasing γ/γ_F leads to trefoils [Fig. 2(f)] and papillons [Fig. 2(g)]. We note that in the range γ/γ_F =0.935–0.95, multiple fundamental orbits may coexist at the same memory, with the dominant three being lemniscates, trefoils, and papillons. The orbits of Fig. 2 are similar to those reported for walkers in the simple harmonic potential.[17,21,22]

At the highest memories considered, $\gamma/\gamma_F = 0.98 - 0.99$, the droplet displays an erratic trajectory similar to that shown in Fig. 2(h), with sudden and seemingly unpredictable variations in speed. At this memory, the motion is characterised by trapped states, in which the droplet bounces in place for a time ranging from 2 to 30 s. These trapping locations can be identified in Fig. 2(h) by their corresponding zero speed. We note that trapped states have also been predicted by Oza *et al.*[36] for motion in a rotating frame at high memory and by Tambasco *et al.*[37] for walkers above the Faraday threshold. Such wave-induced trapping was not reported in the experiments of Perrard *et al.*,[17,18] but was evident in the numerical models of Gilet.[9,10]

In order to provide a more quantitative description of the fundamental trajectories arising for $\gamma/\gamma_F \leq 0.95$, we define the non-dimensional radial distance from the corral centre,

$$R(t) = \frac{r(t)}{\lambda_F}$$

and the non-dimensional angular momentum about the centre,

$$L_z(t) = \frac{\boldsymbol{r}(t)}{\lambda_F} \times \frac{\boldsymbol{V}(t)}{V_0},$$

where $\boldsymbol{r}(t)$ and $\boldsymbol{V}(t)$ are the walker's position and velocity. To be consistent with Perrard *et al.*,[17] we define V_0 as the walker's speed along the first stable trajectory, specifically the small circle shown in Fig. 2(a).

Figure 3 shows the time series of R and L_z over a complete orbital period for the lemniscate, trefoil, and papillon fundamental trajectories evident in Figs. 2(e)–2(g). We note that, while the orbital periods for these 3 fundamental trajectories are different, the time difference between successive radial maxima is comparable. The angular momentum of the lemniscate [Fig. 3(b)] displays a pair of positive and negative peaks of equal magnitude. The angular momenta of the trefoils [Fig. 3(d)] and the papillons [Fig. 3(f)] are either completely positive or negative. The time between successive extrema of the angular momenta is approximately the same for lemniscates, trefoils, and papillons and corresponds to the time between consecutive radial maxima. This common time scale can be understood by noting that the basic unit of time is that of a single loop, with the lemniscate containing 2 loops, the trefoil 3, and the papillon 4.

Following Perrard *et al.*,[17] we characterise the walker's motion by its mean non-dimensional radial distance to the corral centre, $\overline{R}$:

$$\overline{R} = \frac{\sqrt{\langle R^2 \rangle}}{\lambda_F} = \frac{1}{\sqrt{N}} \sqrt{\sum_{k=1}^{N} \frac{r_k^2(t)}{\lambda_F^2}} \tag{1}$$

and its mean non-dimensional angular momentum about the centre, $\overline{L_z}$:

$$\overline{L_z} = \frac{\sqrt{\langle L_z \rangle}}{m \lambda_F V_0} = \frac{1}{N} \sum_{k=1}^{N} \frac{\boldsymbol{r_k}(t)}{\lambda_F} \times \frac{\boldsymbol{V_k}(t)}{V_0}, \tag{2}$$

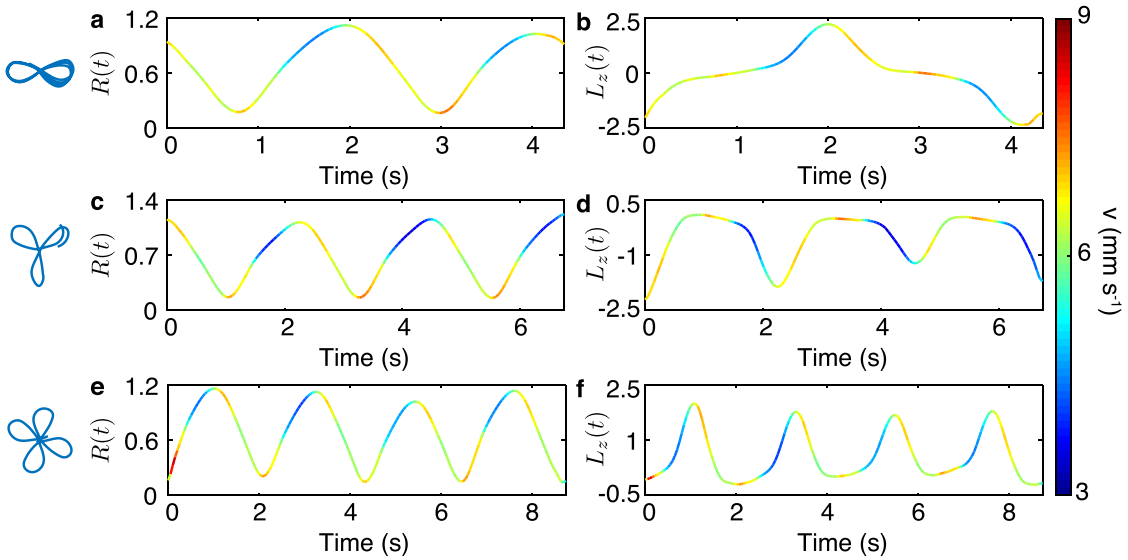

FIG. 3. Time series of radial orbit and angular momentum, colour-coded according to instantaneous drop speed, over one orbital period for [(a) and (b)] a lemniscate, [(c) and (d)] a trefoil, and [(e) and (f)] a papillon. The trajectories analyzed are those highlighted in Figs. 2(e)–2(g).

where $\boldsymbol{r_k}(t)$ and $\boldsymbol{V_k}(t)$ are the walker's position and velocity at the k-th point along the trajectory, N is the total number of points, and m the droplet mass.

Following the method developed by Durey *et al.*,[21] we analyze the motion of the droplet in terms of periodic sub-trajectories by segmenting long trajectories between successive radial maxima. The values of $\overline{R}$ and $\overline{L_z}$ for each such segment are represented by a point in the $\overline{R}-\overline{L_z}$ plane. The next step leverages the use of K-means clustering to calculate the centroids of the global clusters in the $\overline{R}-\overline{L_z}$ space, in order to highlight the double-quantisation in the chaotic regime. We proceed in a similar fashion.

For $0.87 \leq \gamma/\gamma_F \leq 0.95$ [Fig. 4(a)], identifiable clusters representative of double-quantisation are formed by the fundamental trajectories shown in Fig. 2. We note that $\overline{R}$ generally grows with increasing γ/γ_F. While qualitatively similar to the double-quantisation reported for the simple harmonic potential, there are a number of notable differences. For the circular corral, the quantisation in $\overline{R}$ occurs over the range 0.3–0.9, while that in $|\overline{L_z}|$ over the range 0–1.7. By way of comparison, in the simple harmonic potential, the double-quantisation occurs over the ranges $\overline{R}$ =0.4–2.5 and $|\overline{L_z}| = 0 - 1.9$.[22] Hence, a radial compression is apparent: the fundamental orbits arise at lower $\overline{R}$. Furthermore, the lemniscates in the circular corral do not appear in two distinct clusters, resulting in an empty region in the centre of Fig. 4(a). Another difference is that the trefoils in the circular corral are defined by half the value of $\overline{L_z}$ reported for those in the simple harmonic potential. These differences presumably arise owing

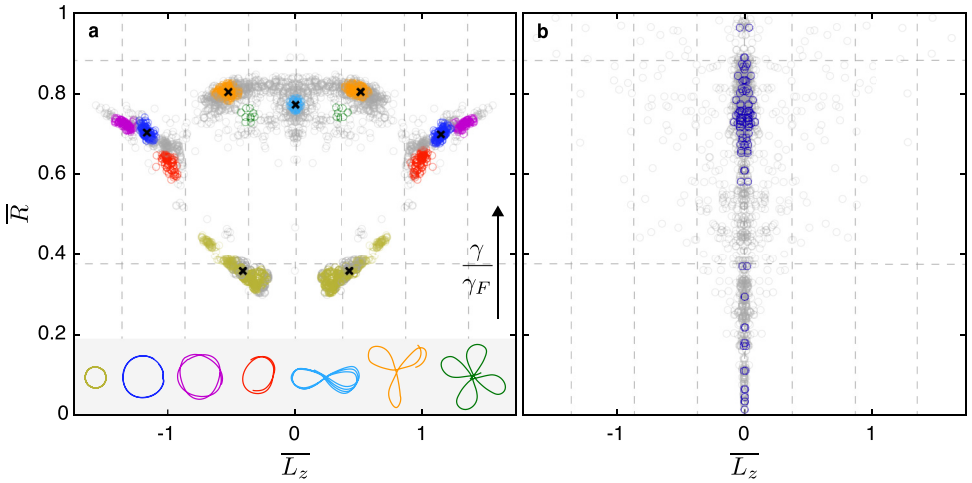

FIG. 4. The double quantisation of angular momentum and orbital radius evident in the circular corral. The axes are the non-dimensional mean angular momentum, $\overline{L_z}$, and the non-dimensional mean radius, $\overline{R}$. Each gray circle represents a separate sub-trajectory. Fundamental trajectories are colour coded to correspond to those shown in Fig. 2. The black crosses are the centroids found via K-means clustering.[21] The data has been symmetrised with respect to $L_z = 0$. The dashed grid has the same spacing as the one used by Perrard *et al.*[17,18] (a) In the intermediate memory regime ($\gamma/\gamma_F = 0.87 - 0.95$), the individual clusters are representative of the stable trajectories identified in Fig. 2. (b) In the high memory regime ($\gamma/\gamma_F = 0.98 - 0.99$), where trajectories are similar to that in Fig. 2(h), the scarcity of clusters with $\overline{L_z} \neq 0$ indicates the dissolution of the double quantisation apparent at lower memory. The blue circles denote walkers in trapped states.

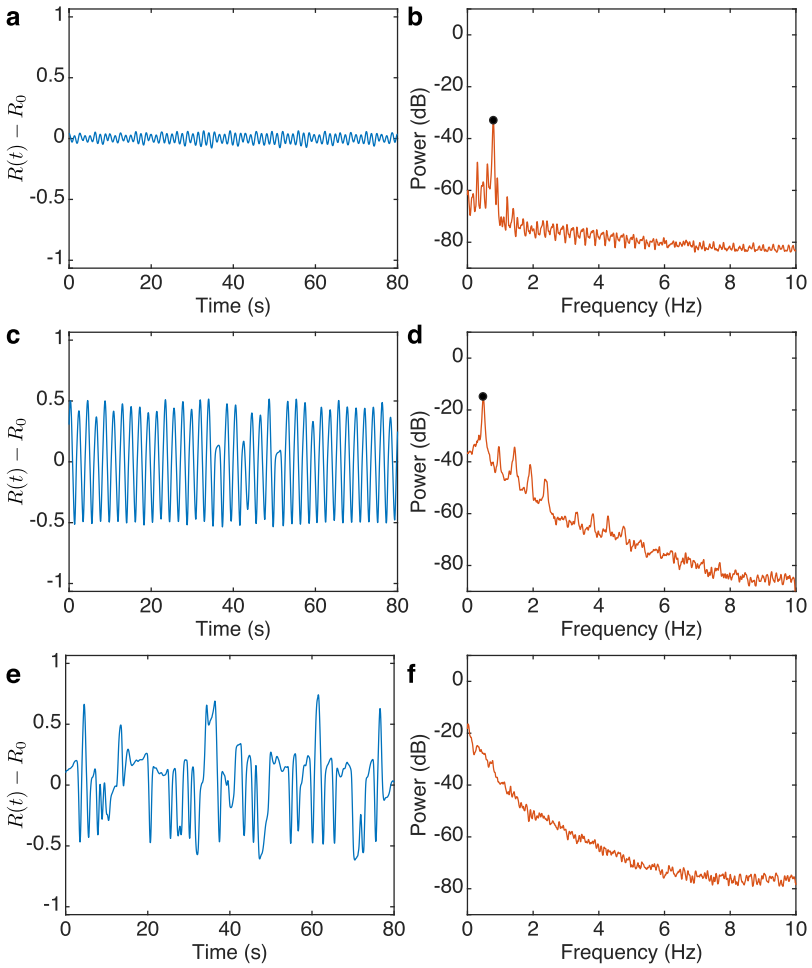

FIG. 5. Walker radial position time series (left column) and associated power spectra (right column) at different memories. The black circles highlight the frequency peaks. [(a) and (b)] $\gamma/\gamma_F = 0.93$, corresponding to the large wobbling circular trajectory shown in Fig. 2(d). [(c) and (d)] $\gamma/\gamma_F = 0.95$, corresponding to the trajectory shown in Fig. 2(g). [(e) and (f)] $\gamma/\gamma_F = 0.98$, corresponding to the trajectory shown in Fig. 2(h).

to the relatively sharp increase in the wall-induced effective potential close to the corral's edges.

For $0.95 < \gamma/\gamma_F < 0.98$, the disappearance of previously identified clusters occurs as the memory is increased, particularly the clusters corresponding to circles and ovals. Some remnants of the lemniscate, trefoil, and papillon clusters are apparent around $\overline{R} = 0.7$ for $|\overline{L_z}| < 0.5$. We notice the emergence of clusters with $\overline{L_z} \approx 0$ having a wide spread in $\overline{R}$.

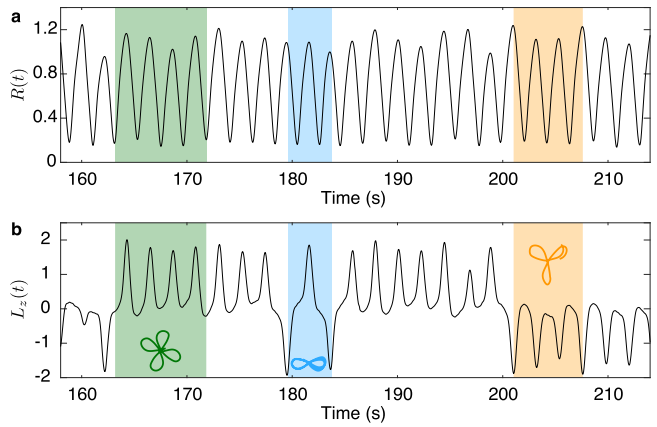

FIG. 6. Time series of (a) orbital radius and (b) angular momentum illustrating chaotic switching between fundamental orbits at $\gamma/\gamma_F = 0.95$. The green shaded area corresponds to a papillon, the blue to a lemniscate, and the orange to a trefoil.

For $0.98 \leq \gamma/\gamma_F \leq 0.99$, no noticeable double-quantisation is apparent [Fig. 4(b)]. Most trajectories are characterised by $\overline{L_z} \approx 0$, an effect due in part to the walker being trapped for extended periods, as is evident in Fig. 2(h). In addition, the erratic trajectories do not typically execute loops, but instead, move along straight lines. We note the preponderance of trapped states at $\overline{L_z} = 0$ and $\overline{R} = 0.7$, denoted by blue circles, indicating the walker's propensity to be trapped[38] at the radius of the unstable large orbit [Fig. 2(c)].

Chaos in the corral

We proceed by characterising the system's transition to chaos that arises as the memory is increased progressively, and stable circular orbits give way to more complex trajectories. Fourier analysis provides a means of characterising the onset of chaos using power spectra.[39,40] A periodic trajectory is defined by a sharply peaked spectrum at one particular frequency as well as a number of higher harmonics.[41] A quasi-periodic trajectory is defined by a sharply peaked spectrum at multiple irrationally related frequencies as well as a number of higher harmonics.[41] A chaotic trajectory is characterised by a broad spectral form.[41]

In Fig. 5, we characterise the evolution with increasing memory of the power spectral form of the droplet radial position $R(t)$ as the circular orbit of radius $R_0 = 0.7$ destabilises into chaos [see Figs. 2(c) and 2(d)]. We note that the circular

orbits found in the range γ/γ_F =0.87–0.93 are stable. Whatever the droplet's initial position, it will eventually converge to such a circular orbit. The left column of Fig. 5 illustrates the time-series of $R(t) - R_0$, where R_0 is the mean radius. The right column shows the associated power spectrum. The black circles highlight sharp peaks in the power spectra. At $\gamma/\gamma_F = 0.93$, the wobbling circles [Fig. 5(a)] give rise to a power spectrum with one sharp peak [Fig. 5(b)].

Figure 5(c) shows the relatively complex time series corresponding to the trajectory in Fig. 2(g) at $\gamma/\gamma_F = 0.95$. The associated spectrum [Fig. 5(d)] shows multiple relatively broad peaks. The dominant peak corresponds to the orbital frequency of a droplet performing a loop, which represents half of a lemniscate, a third of a trefoil, and a quarter of a papillon. The other noticeable peaks are consecutive integer multiples of this dominant loop frequency. Similar plots are obtained for the memory range γ/γ_F =0.935–0.95. In this range, the walker's motion is characterised by chaotic switching between stable subtrajectories, as was also observed in the simple harmonic potential by Perrard *et al.*[17]

Figure 5(e) shows the time-series of a droplet at $\gamma/\gamma_F = 0.98$ with trapped states present and no clear periodic structure. The associated frequency spectrum [Fig. 5(f)] is broad with no distinct peaks. Similar spectral forms arose for larger memories as $\gamma \to \gamma_F$. Our power spectral analysis shows the transition of our system from periodic, to quasi-periodic, to chaotic trajectories as the memory is increased progressively. We note that numerical investigations of the routes to chaos in orbital pilot-wave dynamics indicated that the transition to chaos happens over an extremely narrow range of γ.[24] For example, in the case of a walker in a simple harmonic potential, the transition arose over a span of $\Delta\gamma = 0.004$. Given the limitations in our experimental precision, a detailed characterisation of the route to chaos in corrals was thus impractical. Nevertheless, we have traced the evolution from periodic to quasi-periodic to chaotic trajectories with increasing γ.

Finally, Fig. 6 illustrates the chaotic switching between fundamental trajectories observed at intermediate memories, specifically $\gamma/\gamma_F = 0.95$. Notice the appearance of lemniscates, trefoils, and papillons, as may be identified by their signature time series shown in Fig. 3. Multiple switches between precessing fundamental orbits are a defining feature of the trajectories observed at $\gamma/\gamma_F = 0.95$. This behavior is reminiscent of that reported by Perrard *et al.*,[17] who showed that the chaotic trajectories found experimentally for the simple harmonic potential are characterised by transitions between unstable periodic orbits.

DISCUSSION

Our study serves to connect two hydrodynamic quantum analogs previously considered to be disparate, walker dynamics in a circular corral and in a simple harmonic potential. Both systems are characterised by periodic and quasi-periodic orbits at low memory, and complex chaotic trajectories at high memory. Both systems are characterised by trajectories with preferred radii and angular momenta that lead to a double-quantisation reminiscent of that arising in the quantum simple harmonic oscillator. We have highlighted the similarities and differences between the double quantisation arising here and that reported by Perrard *et al.*,[17] Durey *et al.*,[21] and Kurianski *et al.*[22] for walker motion in a simple harmonic potential. The similarities may be rationalised on the grounds that the corral walls play the role of a relatively sharp confining potential. However, in the high memory regime, the dynamics in the two system are markedly different: the walker in the corral moves erratically between trapped states, presumably owing to the interactions between its pilot-wave and the boundary walls.

Through their influence on the walker wave field, the corral walls act to repel the drop from its edges.[12] One thus expects that the influence of the corral boundaries may be described crudely in terms of a steeply increasing effective radial potential, with a form lying somewhere between a two-dimensional simple harmonic potential and an infinite circular step potential.

Finally, we have examined via power spectra analysis the emergence of chaotic behavior in our system as the memory is increased progressively. Specifically, we tracked the evolution from periodic to quasi-periodic to chaotic behavior. A more detailed characterisation of the route to chaos would be possible by following an approach similar to that of Tambasco *et al.*[24,42] or by building upon the theoretical results of Gilet[9,10] and Rahman and Blackmore.[29] The relation between routes to chaos in the walker system and the pure Faraday wave system[43,44] is also the subject of current interest.

ACKNOWLEDGMENTS

This work was supported by the U.S. National Science Foundation through Grant Nos. DMS-1614043 and CMMI-1727565. The authors thank Yves Couder for motivating this study and Rodolfo Rubén Rosales for valuable discussion.

[1]Y. Couder, S. Protière, E. Fort, and A. Boudaoud, Nature **437**, 208 (2005). ISSN 00280836.
[2]S. Protière, A. Boudaoud, and Y. Couder, J. Fluid Mech. **554**, 85 (2006). ISSN 00221120.
[3]J. W. M. Bush, Annu. Rev. Fluid Mech. **47**, 269 (2015). ISSN 0066-4189.
[4]J. Miles, J. Fluid Mech. **214**, 43 (1990). ISSN 14697645.
[5]A. Eddi, E. Sultan, J. Moukhtar, E. Fort, M. Rossi, and Y. Couder, J. Fluid Mech. **674**, 433 (2011). ISSN 00221120.
[6]D. M. Harris, J. Moukhtar, E. Fort, Y. Couder, and J. W. M. Bush, Phys. Rev. E **88**, 011001(R) (2013). ISSN 15393755.
[7]M. F. Crommie, C. P. Lutz, and D. M. Eigler, Science **262**, 218 (1993). ISSN 0036-8075.
[8]D. Shirokoff, Chaos **23**, 013115 (2013).
[9]T. Gilet, Phys. Rev. E **90**, 052917 (2014). ISSN 15502376.
[10]T. Gilet, Phys. Rev. E **93**, 042202 (2016). ISSN 24700053.
[11]F. Blanchette, Phys. Fluids **28**, 032104 (2016). ISSN 10897666.
[12]G. Pucci, P. J. Sáenz, L. M. Faria, and J. W. M. Bush, J. Fluid Mech. **804**, R3 (2016).
[13]P. J. Sáenz, T. Cristea-Platon, and J. W. M. Bush, Nat. Phys. **14**, 315–319 (2017).
[14]H. C. Manoharan, C. P. Lutz, and D. M. Eigler, Nature **403**, 512 (2000). ISSN 0028-0836.
[15]G. A. Fiete and E. J. Heller, Rev. Mod. Phys. **75**, 933 (2003). ISSN 00346861, 0211607.
[16]C. R. Moon, C. P. Lutz, and H. C. Manoharan, Nat. Phys. **4**, 454 (2008). ISSN 1745-2473, 0904.2884.
[17]S. Perrard, M. Labousse, M. Miskin, E. Fort, and Y. Couder, Nat. Commun. **5**, 3219 (2014).
[18]S. Perrard, M. Labousse, E. Fort, and Y. Couder, Phys. Rev. Lett. **113**, 104101 (2014).

[19]M. Labousse, S. Perrard, Y. Couder, and E. Fort, New J. Phys. **16**, 113027 (2014).
[20]M. Labousse, A. U. Oza, S. Perrard, and J. W. M. Bush, Phys. Rev. E **93**, 033122 (2016).
[21]M. Durey and P. A. Milewski, J. Fluid Mech. **821**, 296 (2017).
[22]K. M. Kurianski, A. U. Oza, and J. W. M. Bush, Phys. Rev. Fluids **2**, 113602 (2017).
[23]A. U. Oza, R. R. Rosales, and J. W. M. Bush, J. Fluid Mech. **737**, 552 (2013).
[24]L. D. Tambasco, D. M. Harris, A. U. Oza, R. R. Rosales, and J. W. M. Bush, Chaos **26**, 103107 (2016).
[25]P. Pierański, J. Phys. France **44**, 573 (1983).
[26]J. Moláček and J. W. M. Bush, J. Fluid Mech. **727**, 582 (2013). ISSN 00221120.
[27]D. Ruelle and F. Takens, Commun. Math. Phys. **20**, 167 (1971). ISSN 1432-0916.
[28]S. Newhouse, D. Ruelle, and F. Takens, Commun. Math. Phys. **64**, 35 (1978). ISSN 1432-0916.
[29]A. Rahman and D. Blackmore, Chaos Solitons Fractals **91**, 339 (2016).
[30]D. M. Harris and J. W. M. Bush, J. Sound Vib. **334**, 255 (2015). ISSN 10958568.
[31]D. M. Harris, T. Liu, and J. W. M. Bush, Exp. Fluids **56**, 83 (2015). ISSN 07234864.
[32]G. Pucci, D. M. Harris, L. M. Faria, and J. W. M. Bush, J. Fluid Mech. **835**, 1136 (2018).
[33]S. Douady, J. Fluid Mech. **221**, 383 (1990). ISSN 14697645.
[34]M. Durey, P. A. Milewski, and J. W. M. Bush, "Dynamics, emergent statistics and the mean-pilot-wave potential of walking droplets," Chaos **28**, 096108 (2018).
[35]J. Moláček and J. W. M. Bush, J. Fluid Mech. **727**, 612 (2013). ISSN 00221120.
[36]A. U. Oza, D. M. Harris, R. R. Rosales, and J. W. M. Bush, J. Fluid Mech. **744**, 404 (2014).
[37]L. D. Tambasco, J. J. Pilgram, and J. W. M. Bush, "Bouncing droplet dynamics above the Faraday threshold," Chaos **28**, 096107 (2018).
[38]N. Sungar, L. D. Tambasco, G. Pucci, P. J. Sáenz, and J. W. M. Bush, Phys. Rev. Fluids **2**, 103602 (2017).
[39]D. Farmer, J. Crutchfield, H. Froehling, N. Packard, and R. Shaw, Ann. N. Y. Acad. Sci. **357**, 453 (1980).
[40]D. Farmer, Phys. Rev. Lett. **47**, 179 (1981).
[41]T. Vialar, *Handbook of Mathematics* (Books on Demand, 2015).
[42]L. D. Tambasco and J. W. M. Bush, "Exploring orbital dynamics and trapping with a generalized pilot-wave framework," Chaos **28**, 096115 (2018).
[43]S. Ciliberto and J. P. Gollub, Il Nuovo Cimento D **6**, 309 (1985).
[44]D. M. Henderson and J. W. Miles, J. Fluid Mech. **222**, 429 (1991).